Finite-size corrections in the Sherrington–Kirkpatrick model

2008 J. Phys. A: Math. Theor. 41 324008

(http://iopscience.iop.org/1751-8121/41/32/324008)

IOP PUBLISHING JOURNAL OF PHYSICS A: MATHEMATICAL AND THEORETICAL

J. Phys. A: Math. Theor. **41** (2008) 324008 (21pp) doi:10.1088/1751-8113/41/32/324008

Finite-size corrections in the Sherrington–Kirkpatrick model

T Aspelmeier[1], A Billoire[2], E Marinari[3] and M A Moore[4]

[1] Max Planck Institute for Dynamics and Self Organization, 37073 Göttingen, Germany
[2] Service de Physique Théorique, CEA Saclay, 91191 Gif-sur-Yvette, France
[3] Dipartimento di Fisica, INFM and INFN, Università di Roma La Sapienza, P A Moro 2, 00185 Roma, Italy
[4] School of Physics and Astronomy, University of Manchester, Manchester, M13 9PL, UK

Received 21 November 2007, in final form 4 February 2008
Published 30 July 2008
Online at stacks.iop.org/JPhysA/41/324008

Abstract

We argue that when the number of spins N in the Sherrington–Kirkpatrick model is finite, the Parisi scheme can be terminated after K replica-symmetry breaking steps, where $K(N) \propto N^{1/6}$. We have checked this idea by Monte Carlo simulations: we expect the typical number of peaks and features R in the (non-bond averaged) Parisi overlap function $P_J(q)$ to be of order $2K(N)$, and our counting (for samples of size N up to 4096 spins) gives results which are consistent with our arguments. We can estimate the leading finite-size correction for any thermodynamic quantity by finding its K-dependence in the Parisi scheme and then replacing K by $K(N)$. Our predictions of how the Edwards–Anderson order parameter and the internal energy of the system approach their thermodynamic limit compare well with the results of our Monte Carlo simulations. The N-dependence of the sample-to-sample fluctuations of thermodynamic quantities can also be obtained; the total internal energy should have sample-to-sample fluctuations of order $N^{1/6}$, which is again consistent with the results of our numerical simulations.

PACS numbers: 75.50.Lk, 75.10.Nr, 75.40.Gb

(Some figures in this article are in colour only in the electronic version)

1. Introduction

The Sherrington–Kirkpatrick (SK) [1] model of spin glasses has been the subject of hundreds of papers. It is the model for which a mean-field theory becomes exact in the thermodynamic limit (i.e. when N, the number of spins in the model, becomes infinite). Parisi's replica-symmetry breaking (RSB) solution [2] is now known to be the correct mean-field solution [3]. Extensive studies, mostly numerical, have been made of the model at finite N values. Analytically, the determination of the properties of the model at finite N—the finite-size corrections—is a much more challenging task in the low-temperature phase than finding the

mean-field theory. At finite N all the loop corrections to the mean-field solution need to be considered. Because of the massless modes present in the low-temperature phase [4] each term in the loop expansion is infinite. Hence, a direct perturbative approach is impossible. A similar situation applies in finite-dimensional spin glasses, already for the bulk term, when the dimension d is smaller than 6 [5], so that one could hope at least that experience gained in studying finite-size effects in the SK model might be relevant to spin glasses in physical dimensions.

Unfortunately, we have been unable to find any systematic theoretical treatment of the finite-size problem. However, we have managed to obtain insights into it by examining the structure of the Parisi overlap probability distribution function $P_J(q)$ (i.e. *the non-averaged overlap probability distribution function*) at finite N values. $P_J(q)$ is defined as the probability that the overlap of the spins in two copies of the system with the same realization of the quenched disorder J_{ij} is equal to q, i.e.

$$P_J(q) \equiv \left\langle \delta\left(q - \frac{1}{N}\sum_i \sigma_i \tau_i\right)\right\rangle, \tag{1}$$

where the Hamiltonian of the two-copy system is

$$\mathcal{H} = -\sum_{\langle ij\rangle} J_{ij}(\sigma_i\sigma_j + \tau_i\tau_j), \tag{2}$$

and the sum runs over all the pairs ij of sites in the system. The thermal average $\langle\cdots\rangle$ in equation (1) is taken over the Boltzmann weight associated with all the possible values (± 1) of the Ising spins σ_i and τ_i. It has been known for many years that the function $P_J(q)$ is very different for different realizations of the bonds. In particular it contains a very variable number R of peaks, humps or shoulders. In this paper, we shall systematically study the distribution of R and the dependence of its average on the number of spins N. We shall give numerical and analytic arguments that the mean number of features R increases as N^μ, with $\mu = 1/6$ and that δR, the width of the distribution of R, is N independent for large N. The next step of our approach is to argue that the Parisi replica-symmetry breaking scheme, which involves K levels of symmetry breaking (where in order to achieve a stable solution K has to be taken infinite in the thermodynamic limit), is stabilized at finite N at a value $K(N)$ by self-energy contributions (whose N-dependence is estimated in appendix A). As a consequence we can estimate K for a given system size and because $R = 2K$ (see section 8) we can understand the size dependence of the number of peaks/features in $P_J(q)$.

The next step towards predicting the exponents which give the leading N-dependence of the corrections to the thermodynamic limit of quantities such as the internal energy per spin e is simply to use the RSB scheme to compute the dependence of the quantity on K. For example $e = e_P + O(K^{-4})$, where e_P denotes the value of the internal energy in the infinite K limit [6]. Our prescription for evaluating the exponents of the leading finite-size corrections is to set $K = K(N) \sim N^{1/6}$; this implies that the leading finite-size correction to the thermodynamic limit of the internal energy per spin should be of order $N^{-2/3}$. Since arguments of this type do not have the strength of a theorem and can only be suggestive of the possible behaviour, we have checked our arguments with extensive Monte Carlo simulations. We have computed many quantities at a number of different values of the temperature. Our results for the internal energy are reported in section 6. These data support the value of $2/3$ predicted by our approach for the exponent of the leading finite-size correction.

Similarly, the Edwards–Anderson order parameter q_{EA} at finite K differs from its infinite K form by a term of order K^{-2}. Hence we predict that the finite-size shift of q_{EA} should be of $O(1/N^{1/3})$, and we present numerical evidence for this behaviour in section 9.

Our approach can be used to investigate the sample-to-sample fluctuations of any quantity by relating them to the sample-to-sample variation in the number of features in $P_J(q)$, δR. For the internal energy we shall find in section 7 numerical evidence consistent with this approach, together with a discussion of the behaviour of the sample-to-sample fluctuations in the critical regime and in the high-temperature phase. Our basic prediction is that the sample-to-sample fluctuations in the total free energy of a system of N spins are of order N^{Υ} where the exponent $\Upsilon = \mu = 1/6$. There have been numerous attempts to determine this exponent, both numerically and analytically, and we also review them in section 7.

Because the peaks/features in $P_J(q)$ are caused by the overlap of pure states, in particular those states whose free energies are of order $k_B T$ from that of the lowest free energy state, one can relate the number of these pure states to the number of peaks R using the relation $R = 2K$. This connection is simplified because of the ultrametric organization of states in the SK model and the details of the argument are given in section 8. In section 9, we discuss the relation of these ideas with the behaviour of finite-dimensional spin glasses.

2. Theoretical framework

Our Monte Carlo studies of the Parisi overlap probability distribution function $P_J(q)$ for systems of N spins (with N up to 4096) show that the number R of peaks/features is usually quite small and that it increases only slowly with N, apparently as $R \sim N^{\mu}$, with $\mu \approx 1/6$. Our approach to the study of finite-size effects in the SK model is to argue that R, the average number of such peaks/features for a system of size N, can be connected to a truncation of Parisi's RSB scheme at its Kth step, with $R = 2K(N)$.

The Parisi scheme at the Kth level of RSB parametrizes the bond average of $P_J(q)$, $P(q)$, by a series of delta functions at various values of q, namely $q_1, q_2, \ldots, q_K$:

$$P(q) = \sum_{i=1}^{K} a_i \delta(q - q_i). \tag{3}$$

The weights of the delta functions a_i and their positions q_i are the variational parameters that one optimizes to obtain the Parisi solution. In the thermodynamic limit, where N goes to infinity, a Parisi RSB solution with $K > 1$ is only stable if K is taken to infinity. We argue that in finite-size systems the self-energy corrections to the Parisi solution can stabilize an RSB solution with a finite value of K, and we will argue that $R = 2K \sim N^{\mu}$. (In zero field $P_J(q) = P_J(-q)$ so the number of peaks/features $R = 2K$. However, if q_1 just happens to be zero, i.e. there is a peak at the origin, then $R = 2(K-1)+1 = 2K-1$.)

Consider the single-valley replicon correlation function $G_R(i,j) = \overline{\langle S_i S_j \rangle_c^2}$. At wavevector $\mathbf{k}$ its Fourier transform takes the form described in [4], and at Gaussian order, $G_R(k) = 1/k^2$, both for $T < T_c$ and $T = T_c$. (Strictly speaking in the SK model the only possible value which k can take is zero, but we will find it useful to consider non-zero values of k.) Right at $k = 0$, $G_R(0)$ is infinite in the thermodynamic limit. For finite N, the self-energy corrections neglected at Gaussian order will be shown in appendix A to produce a divergence growing as $N^{1/3}$. Schematically

$$G_R(k) = \frac{1}{k^2 + \Sigma_R}, \tag{4}$$

so that the self-energy Σ_R is of order $1/N^{1/3}$.

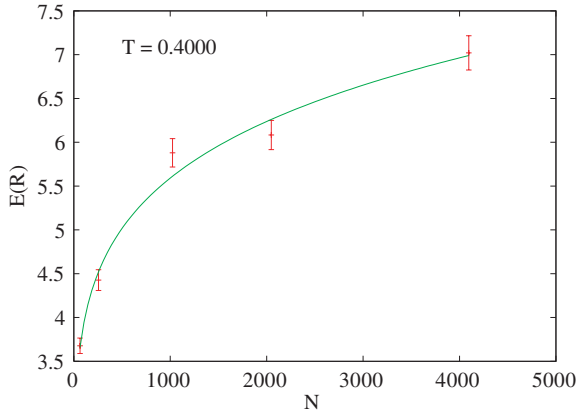

Figure 1. Scaling plot of $E(R)$ (the average number of peaks/features determined by visual inspection of the individual $P_J(q)$) as a function of N, for $T = 0.4$. The curve is the best fit to the form $E(R) = a + bN^c$ with $c = 0.17 \pm 0.14$.

Now for finite values of K in the Parisi RSB scheme, the Gaussian propagator is unstable and behaves as [6]

$$G_R(k) = \frac{1}{k^2 - \frac{4}{3}\frac{t^2}{(2K+1)^2}}, \tag{5}$$

in the regime near the transition temperature T_c where $t \equiv 1 - T/T_c$ is small. The instability at $k = 0$ only disappears when one takes the infinite K limit. Our basic idea is that for finite N this instability can be removed by the stabilizing effect of the self-energy Σ_R. Then if $\Sigma_R = c/N^{1/3}$ stability will be achieved when

$$\frac{4}{3}\frac{t^2}{(2K+1)^2} \sim c/N^{1/3}. \tag{6}$$

In other words, when $K = K(N) \sim tN^{1/6}$, there will be no need to break the symmetry further (at least to achieve stability). This would explain why the number of peaks/features in $P_J(q)$ increases as $N^{1/6}$ (see figure 1).

Our procedure to determine the finite-size corrections to scaling of any thermodynamic quantity proceeds in a similar fashion. First one obtains from RSB calculations the Kth approximation for the quantity. Thus the free energy per spin below but near T_c is to order t^5, and at large values of K [6]

$$\Delta f = \left(\frac{1}{6}t^3 + \frac{7}{24}t^4 + \frac{29}{120}t^5\right) - \frac{1}{360}t^5\left(\frac{1}{K}\right)^4. \tag{7}$$

The same kind of dependence $\sim K^{-4}$ of the excess term has been found at $T = 0$ by Oppermann *et al* [7]. To estimate the N-dependence of the finite-size corrections we replace K by $tN^{1/6}$. This gives a term in Δf which scales as $t/N^{2/3}$, which is in excellent agreement with numerical studies [8]. Just as the self-energy corrections to equation (5) change the sign of $G_R(0)$, we would expect that the higher loop corrections to the free energy will also change the sign of this correction, but not its N-dependence.

A similar argument can be given for other quantities. The additional terms in the internal energy per spin below T_c at order K in the RSB procedure are [6]

$$\Delta u = \left(\frac{1}{2}t^2 + \frac{5}{6}t^3 + \frac{1}{3}t^4\right) - \frac{1}{72}t^4\left(\frac{1}{K}\right)^4. \tag{8}$$

Substituting as before $tN^{1/6}$ for K, the finite-size corrections to the internal energy would be expected to be of order $1/N^{2/3}$.

The Edwards–Anderson order parameter [6] is to order K

$$q_{\mathrm{EA}} = t + t^2 - \frac{2}{3(2K+1)^2}t^2, \tag{9}$$

correct to order t^2. It is thus to be expected on substituting for K that the finite-size corrections to q_{EA} are of order $1/N^{1/3}$. If one defines q_{EA} for finite-size systems as the value of q at which the Parisi overlap function $P(q)$ peaks, then such an N-dependence is in excellent agreement with both existing numerical and theoretical arguments [9]. We postpone to section 9 the comparison with the results of our numerical analysis of the scaling behaviour of q_{EA}.

Our approach can be extended to determine the N-dependence of sample-to-sample fluctuations of, say, the internal energy or the free energy. In [10] it was shown that the variance of the sample-to-sample fluctuations of the extensive free energy δF varies as a quantity $-J(0)$, which at Gaussian order has the property $-J(k) \approx k^{-2}$. At finite RSB of order K, an exact expression for this quantity was given in [11]. As shown in appendix B, it can be evaluated when k^2 (which is originally a wave vector) is replaced by the self-energy. One gets that

$$-J \approx N^{1/3} f(t), \tag{10}$$

where $f(t)$ is some known function (see appendix B). This shows that the variance of δF is of order $N^{1/3}$, with typical fluctuations being of order $N^{1/6}$.

From this result one can compute the sample-to-sample fluctuations of R. To do this we shall suppose that the sample-to-sample fluctuation of K is of order δK. Then equation (7) implies that the sample-to-sample fluctuation of the extensive free energy δF behaves as

$$\delta F \sim N t^5 \left(\frac{1}{K}\right)^5 \delta K. \tag{11}$$

Given that $\delta F \approx N^{1/6}$, it follows that δK is of $O(1)$, that is independent of N.

We have determined the sample-to-sample fluctuations of the internal energy in the course of our simulations, and their N-dependence can be predicted by extension of these arguments. From equation (8), the sample-to-sample variation of the full internal energy δU is

$$\delta U \approx N t^4 \left(\frac{1}{K}\right)^5 \delta K. \tag{12}$$

Substituting for K and δK, it follows that $\delta U \approx t^{-1} N^{1/6}$. These sample-to-sample fluctuations appear to diverge at $T = T_c$, but equation (8) only holds in the RSB region, which is outside the critical regime (which is defined by the limits $N \to \infty, t \to 0$, with Nt^3 fixed [12]).

All these arguments are intuitive rather than rigorous. As a consequence, we have attempted to check them by numerical simulations of the finite-size SK model.

3. The Monte Carlo simulation

We have based our analysis on a large set of numerical data produced by the large scale parallel tempering simulation of [13, 14], supplemented by a new large scale simulation for lattices with $N = 2048$ spins.

Table 1. The relevant parameters of our numerical runs: number of sites N, number of parallel tempering sweeps used for measurements N_{meas}, number of parallel tempering sweeps used for thermalization N_{equi} and number of disorder samples N_J.

N	N_{meas}(K)	N_{equi}(K)	N_J
64	1000	400	1024
128	1000	400	8192
256	1000	400	1024
512	200	200	1024
1024	1000	400	1024
2048	200	200	512
4096	500	400	256

The quenched random couplings of our system can take the two values ± 1 with equal probability; the use of such binary couplings allows us to write computer codes that run much faster than, say, when using quenched random couplings assigned under a Gaussian distribution. We assume that the interesting leading scaling behaviour is the same, for example, when using binary or Gaussian couplings.

We report in table 1 the relevant parameters of our numerical simulations. The temperatures allowed to the parallel tempering steps are in the range $T \in [0.4, 1.3]$.

A parallel tempering sweep consists of one Metropolis sweep (all spins are updated in lexicographic order) followed by a temperature exchange sweep (we try to exchange adjacent values of T in sequential order). The balance between the number of sweeps performed for each disorder sample and the number of disorder samples included has been chosen cautiously in order to avoid any possible bias due to a non-perfect thermalization; we have chosen a safe compromise favouring, at fixed amount of computer time, the number of sweeps over the number of disorder samples. We have checked the quality of thermalization by monitoring for example the value of q^2 as a function of the Monte Carlo time, starting from an ordered initial spin configurations (all spins equal to one). For all values of T and N the disorder averaged data do not drift appreciably already after a couple of thousand sweeps, i.e. far before we start taking measurements. A second important test is provided by the symmetry of the individual $P_J(q)$'s that is very good for most samples (see section 4). In practice, we found that at temperatures $T < 0.4$ it was difficult to equilibrate our larger samples. However, we also wish to disentangle our finite-size effects from critical fluctuations so most of our analysis were carried out at $T = 0.4$, i.e. well below the critical temperature $T_c = 1$.

In the rest of this paper we will denote by $E(\cdots)$ the average over the quenched disorder, $U = Ne$ the total internal energy and $\delta U = N\Delta$ its standard deviation, with $N^2\Delta^2 \equiv E(U^2) - E(U)^2 = N^2(E(e^2) - E(e)^2)$.

4. The structure of $P_J(q)$

As mentioned before, the function $P_J(q)$ is very different for different realizations of the bonds. Figure 2 shows eight such distributions for the lowest temperature value ($T = 0.4$) of the largest system ($N = 4096$) we have simulated. The symmetry of the plots under inversion of the overlap is excellent: one can see that even very small peaks appear with their reflected counterpart, and this is a remarkable check of good thermalization. The only mild asymmetries one can see concern the peaks heights, connected to the population of the different 'pure states to be', that is a very difficult quantity to estimate by Monte Carlo integration (just think about the two peaks in the magnetization distribution for the usual Ising model in three dimension

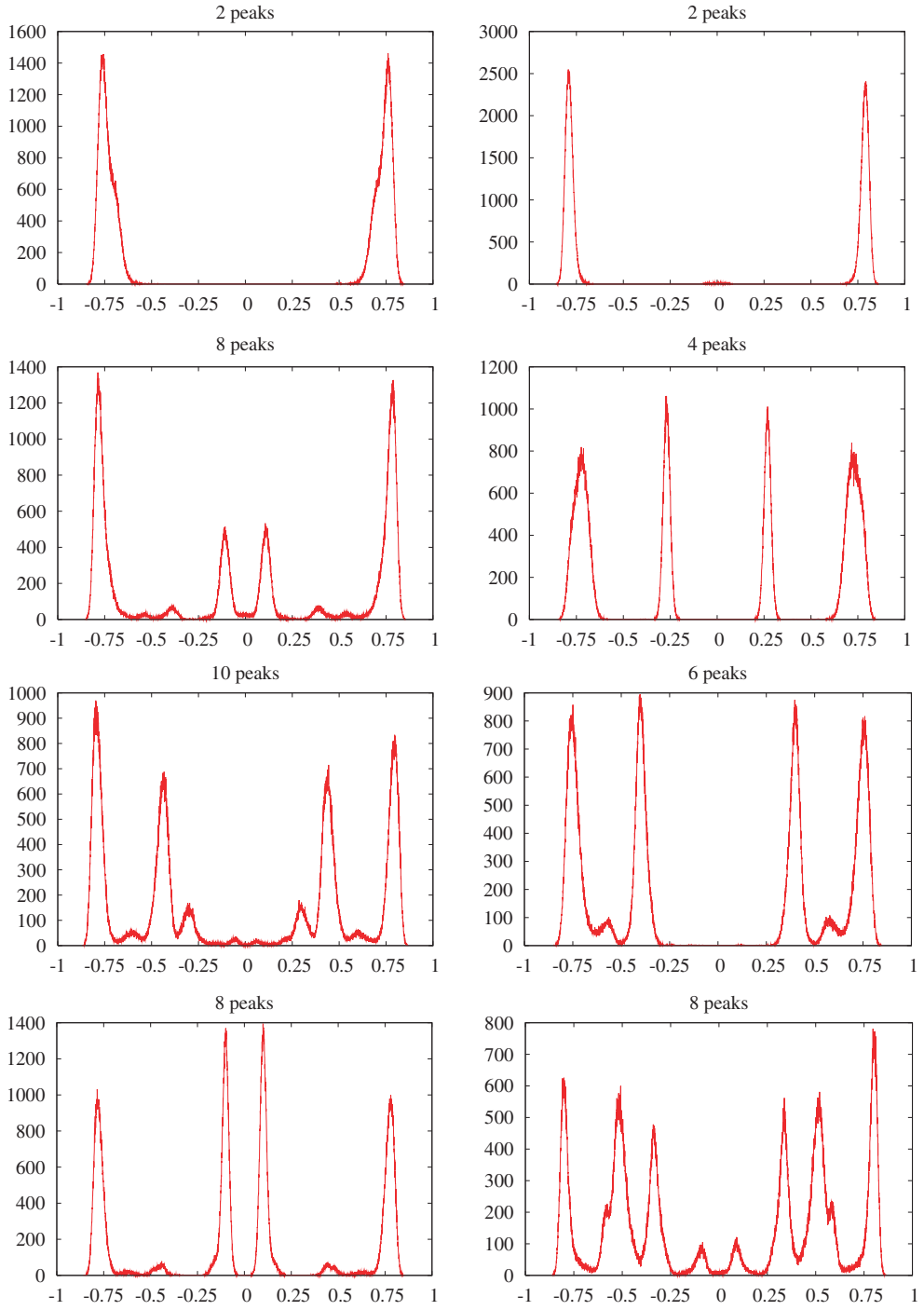

Figure 2. $P_J(q)$ for eight different disorder realizations: here $N = 4096$ and $T = 0.4000$. Those are the first eight disorder configurations generated by our computer program. The symmetry of the plots around $q = 0$ is a good test of thermalization. The number of peaks R quoted above each figure is the value computed by our computer program.

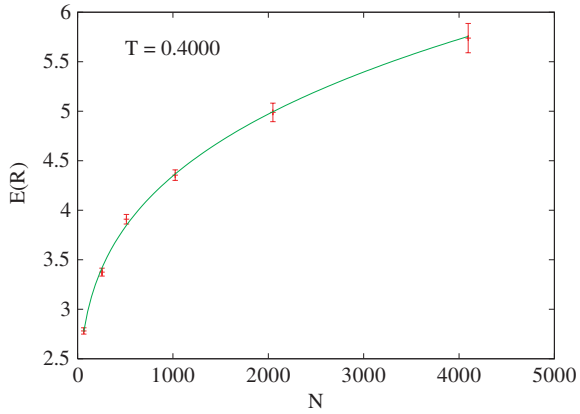

Figure 3. Scaling plot of $E(R)$ determined by automatic peak counting, as a function of N, for $T = 0.4$. The curve is the fit to the form $E(R) = a + bN^c$ with $c = 0.28 \pm 0.04$.

below the Curie temperature). Each of P_J exhibits a given number R_J of features (well-formed peaks, humps, shoulders on the side of a peak and so on) that we are interested to determine in order to compute its disorder expectation value $E(R)$ and the scaling behaviour of $E(R)$ with N.

Peaks/feature counting is not at all a trivial issue when dealing with noisy data. The first assumption must be that the statistical accuracy of the data set is good enough not to hide important features (in this respect it is possible that further improvements to the Monte Carlo scheme could help: one could check for example if using multi-overlap algorithms [15, 16] could be of help). Under this assumption we have developed a computer code that counts the number of peaks. The first step is based on smoothing up the (symmetrized) data for $P_J(q)$. The second step determines the peaks of the smoothed data: the peaks are defined as local maxima of $P_J(q)$ where a valley at least lower than a percentage p of the peak height follows the peak on both sides (we have selected $p = 90\%$ and we have relaxed the depth condition for valleys that include one of the two frontiers of the support, i.e. $q = \pm 1$). As a third and last step we impose a cutoff on the putative peak heights: we discard any peak of height lower than 1% of the highest peak present in $P_J(q)$ for the given disorder sample. In what follows, we will call 'automatic peak counting' this procedure to determine features.

We did not push the coding to include in our automatic peak counting the more complex structures which visual inspection spots: an automatic approach to such a complex task needs great care to avoid arbitrary choices that could lead to misleading conclusions.

For example, it looks clear that the first plot of figure 2 (the upper-left figure) is characterized by four features, two for $q > 0$ and the two symmetric ones for $q < 0$. The first feature is the clear peak that the computer code also finds, while the second very clear feature is the shoulder on the peak: this shoulder is naturally interpreted as a second unresolved peak, too wide to be an isolated feature, but whose presence is very clear to the observer. In other words, it is clear that a correct analysis of this feature would lead to $R = 4$ and that the conclusion $R = 2$ reached by our computer code is not careful enough. To be on the safe side, we have carried out the tedious task of looking at the first $192 P_J(q)$'s for $T = 0.4$ and estimating by eye the number of features R for every graph. This procedure will be called 'visual inspection' in what follows.

We show the behaviour of $E(R)$ as a function of N for $T = 0.4$ in figure 1 for the visual inspection and in figure 3 for the automatic peak counting. The statistical errors are estimated

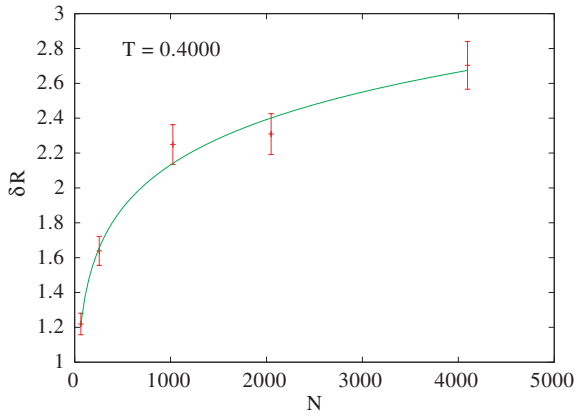

Figure 4. Scaling plot of δR determined by visual inspection, as a function of N, for $T = 0.4$. The curve drawn is a fit to the form $\delta R = a + bN^c$. The best fit is obtained for $c = 0.07 \pm 0.13$.

from the fluctuations between the disorder samples. Our visual inspection gives on average between one and two extra features that are not found by the automatic computer counting. This only means that there are in average between one and two extra features that are not simple peaks. The best fits to the form $E(R) = a + bN^c$ for the two cases give the exponents $c_{\text{visual}} = 0.17 \pm 0.14$ for the visual inspection and $c_{\text{automatic}} = 0.28 \pm 0.04$ for the automatic count. The difference between the estimated error bars mainly reflects the number of disorder samples considered in the two cases. Our prediction is $c = 1/6 \approx 0.17$. Our result for c_{visual} is on the top of it but it has a huge statistical error, while our result for $c_{\text{automatic}}$ is not consistent with $1/6$ at more than two standard deviations (but is of uncertain relevance). It is important to note that here we are dealing with a quantity that grows very slowly and is very small even for our largest systems, and that pre-asymptotic effects could be large.

In figure 4 we show

$$\delta R \equiv [E(R^2) - E(R)^2]^{1/2}, \tag{13}$$

i.e. the fluctuations of R (as determined by visual inspection), together with the best fit to the form $\delta R = a + bN^c$. The best fit is obtained for $c = 0.07 \pm 0.13$: our theoretical estimate in section 2 of the value of the exponent c was zero; our numerical work is consistent with this estimate, although greater precision is really needed before the result can be regarded as definitive.

In conclusion, we cannot claim to have good numerical evidences for $R \sim N^{1/6}$ and $\delta R \sim N^0$, but our data are consistent with this predictions.

In figure 5 we give the empirical distribution of the number of features R obtained by visual inspection for $N = 4096$ and $T = 0.4$: the distribution is very wide. It is also clear from the figure that even values of R are more common than odd values: this is expected, since odd values are only obtained in cases where $P_J(q)$ has a peak in $q = 0$.

5. Finite-size shift in the energy

In figure 6, we show the internal energy per spin as a function of $N^{-2/3}$ for our lowest temperature $T = 0.4$ (that we believe is low enough to be free of effects from the critical point). The statistical errors are again estimated from the fluctuations between the disorder samples.

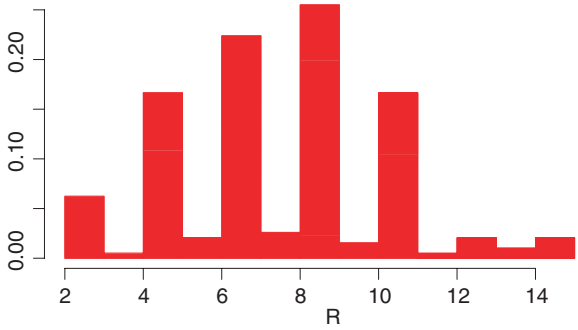

Figure 5. Distribution of the number of features R obtained by visual inspection for $N = 4096$ and $T = 0.4$.

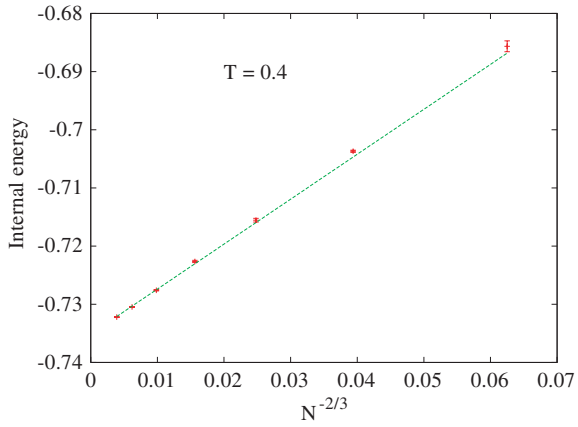

Figure 6. The internal energy as a function of $N^{-2/3}$ for $T = 0.4$. The line is a linear fit (using data for $N \geqslant 256$) as a function of $N^{-2/3}$ to the data.

In the same figure we show a fit to the form $e_N = e_\infty + AN^{-2/3}$, using the value $e_\infty = -0.735\,110\,726$ from [17]. The best fit is obtained for $A = 0.77 \pm 0.01$, with a χ^2 of 12 for 4 degrees of freedom. The presence of slow decaying sub-leading corrections (the dominant sub-leading contribution behaves like $1/N$, barely faster than $N^{-2/3}$) explains presumably why χ^2 is larger than the number of degrees of freedom. The importance of the corrections to the leading behaviour (together with some statistical oddness) is shown in figure 7, where we plot $N^{2/3}(e_N - e_\infty)$ as a function of $1/N^{1/3}$: this is a way to focus on the deviations from the leading behaviour. We do believe that the three leftmost odd looking data points in figure 7 are due to a statistical fluctuation. The curve is a fit to $N^{2/3}(e_N - e_\infty) \propto 1/N^{1/3}$, which is the form we would expect from a $1/N$ correction to the internal energy per spin. Based on figures 6 and 7 we conclude that our numerical data are consistent with an exponent $2/3$ at $T = 0.4$. Other temperatures were studied in [19] (see figure 11 of that paper) and it is our conclusion that the numerical data are consistent with $2/3$ in the whole spin glass phase, although the work of [19] indicates that at some temperatures finite-size corrections are substantial. We disagree with the conclusions of [18] that are based on data with $36 \leqslant N \leqslant 196$, namely a region that is discarded altogether in our fits (see [19] for a detailed comparison). On the other hand, our results agree perfectly with the data shown in [20, 26–29] for the SK model and in [21] for the Bethe lattice, both obtained at $T = 0$.

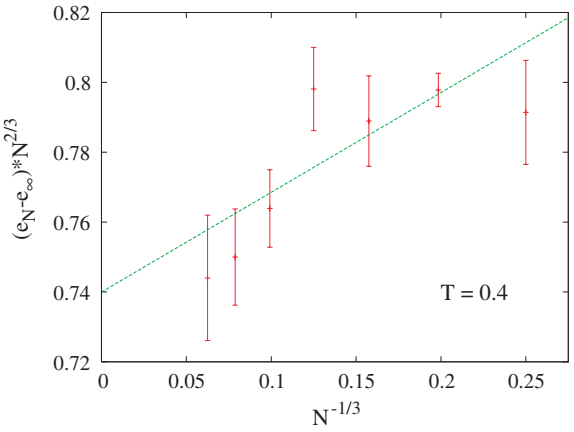

Figure 7. $N^{2/3}(e_N - e_\infty)$ as a function of $N^{-1/3}$ for $T = 0.4$. The line is a linear fit (all data points are included) to the data, of the form $A + BN^{-1/3}$.

6. The Edwards–Anderson order parameter q_{EA}

We have studied the finite-size behaviour of the Edwards–Anderson order parameter q_{EA}, improving the analysis of [9]. We define q_{EA} on a finite system as the location of the maximum of the disorder averaged $P(q) = E(P_J(q))$. The exact procedure is the following: we first symmetrize our data for $P(q)$, then we determine the maximum value reached by the function (we call it $P_{\max}$) and finally we compute q_{EA} by means of a quadratic fit of the data in the range of positive q values such that $P(q) > 0.95P_{\max}$, using the same weights for all data points. This gives us an estimate of $q_{\mathrm{EA}}(N)$ that is not forced to take discrete values: statistical errors are obtained through a jackknife analysis (obviously a jackknife approach would not make sense if q_{EA} was constrained to take discrete values).

We have compared the values we have obtained for q_{EA} to values obtained with shorter numerical simulations, and there is an excellent agreement: this strongly suggests that the procedure we have used to determine $q_{\mathrm{EA}}(N)$ has no appreciable statistical bias. We show in figure 8 our data for $q_{\mathrm{EA}}(N)$ as a function of $N^{-1/3}$ for $T = 0.4$, together with our best fit (using data with $N \geqslant 256$) that uses the infinite volume result $q_{\mathrm{EA}} = 0.759$ from [17]. The value of χ^2 is 10 for 4 degrees of freedom. The small N data exhibit larger corrections from the asymptotic behaviour than those for the internal energy. This is not unexpected since the definition of q_{EA} on a finite system is involved: for example the intrinsic resolution of the determination of q_{EA} in a finite system is $2/N$ (that is close to 0.03 for $N = 64$), a value that is exactly on the scale of the deviations that we observe.

7. The sample-to-sample fluctuations of the internal energy

We have also analysed the fluctuations of the internal energy between different bond realizations using as a measure

$$\delta U^2 = N^2\big(E\big(\langle e\rangle_J^2\big) - E(\langle e\rangle_J)^2\big). \tag{14}$$

The issue of the scaling behaviour of the free energy fluctuations in the SK model has been investigated intensively over the years. Let us define an exponent Υ by the equation

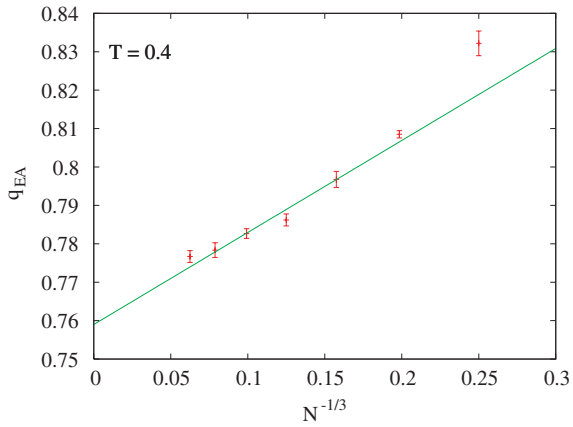

Figure 8. The Edwards–Anderson order parameter $q_{\mathrm{EA}}(N)$, as defined in the text; here $T = 0.4$. The line is for the best fit to the data as a linear function of $N^{-1/3}$ (for $N \geqslant 256$).

$$\delta F^2 = N^2\left(E\left(\langle f\rangle_J^2\right) - E(\langle f\rangle_J)^2\right) \sim N^{2\Upsilon}. \tag{15}$$

Our theoretical approach suggests that Υ should be $\mu = 1/6$. The first investigation we know is the numerical work of [22] at $T = 0$ which gave (on very small samples) the result $\Upsilon = 0.222$, compatible with $\Upsilon = 1/4$. The later theoretical analysis of [23] gives $\Upsilon = 1/6$. However, there is a caveat to this conclusion. What is effectively calculated is the tail of the probability distribution of the free energy on the low-free energy side [24]; and in order to get Υ one has to assume that the N-dependence of the fluctuations in the tail equals that of the standard deviation of the free energy. Ultimately these analyses relate the value of Υ to the order of the first nonlinear term in the expansion of the replicated free energy in powers of n (the number of replicae), which is the n^6 term [4]. More recently, several authors, using exact or heuristic ground states determination algorithms, have found zero temperature values compatible [20, 25–29] with $\Upsilon = 1/4$, some excluding [25, 26, 20, 28] the $\Upsilon = 1/6$ value, some not [27, 29]. Analytical arguments in support of the $\Upsilon = 1/4$ value can be found in [27, 30]. Finally, a recent analytical work [31] using an innovative method obtains the exact bound $\Upsilon \leqslant \frac{1}{4}$ in the low T phase. Clearly, the situation is far from being settled. It should be clear that in the numerical approach it is extremely hard to distinguish with confidence exponents as close as $1/4$ and $1/6$ when the range of variations of N is small (typically one decade), the more so as the functional form of the next correction is unknown. A further difficulty is that exact algorithms are limited to very small systems and heuristic algorithms are heuristic.

The above results are for the free energy. The problem for the internal energy at finite temperature has never, to our knowledge, been studied numerically; we will consider here finite, low-temperature values, and this will allow us to analyse both the low T phase and the $T \to 0$ limit.

Let $\tilde{e}_J$ be the energy measured at some temperature T during the numerical simulation of a system with a given realization of the disorder J (this is what we call a sample of our system). $\tilde{e}_J$ comes from the average of N_{meas} values, and we can use the quantity

$$\left[\frac{1}{N_J}\sum_J \tilde{e}_J^2 - \left(1/N_J \sum_J \tilde{e}_J\right)^2\right], \tag{16}$$

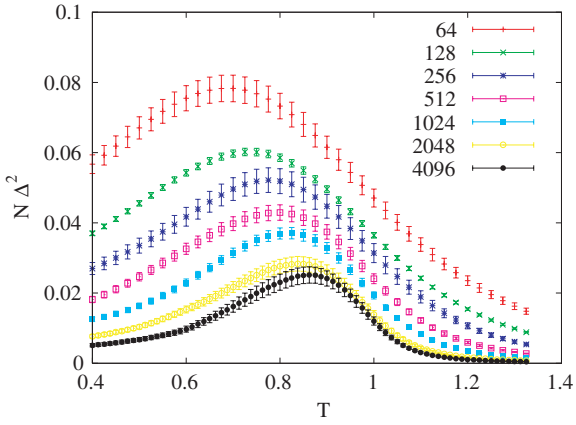

Figure 9. The energy fluctuation $\delta U^2/N = N\Delta^2(T)$ as a function of T, for different values of N.

where N_J is the number of samples, to estimate

$$\Delta^2(T) = E(\langle e^2\rangle_J) - E(\langle e\rangle_J)^2. \tag{17}$$

At leading order $\Delta^2(T)$ and δU^2 are related through

$$\Delta^2(T) = \frac{\delta U^2}{N^2} + \frac{2\tau_{\rm int}^{(E)} T^2 C_N(T)}{N_{\rm meas} N}, \tag{18}$$

where $\tau_{\rm int}^{(E)}$ is the integrated autocorrelation time for the energy at temperature T, $C_N(T)$ is the specific heat and $N_{\rm meas}$ is the number of parallel tempering sweeps performed during the measurement phase of the simulation (we measure the energy after every Metropolis sweep of the system).

It turns out that in our numerical data the second term in equation (18) is negligible, as we have checked by comparing the estimates of $\Delta^2(T)$ in different numerical simulations for the same set of disorder couplings (with $N = 64\,256$ and 1024) using the first 200 K parallel tempering (PT) sweeps and the second 1000 K PT sweeps after thermalization. To the best of our knowledge, the autocorrelation time $\tau_{\rm int}^{(E)}$ of the parallel tempering algorithm has never been measured for the SK model, and our results show that it is very small. Our results for $\Delta^2(T)$ as a function of T can be found in figure 9.

Figure 10 shows the scaling behaviour of δU for our lowest temperature. The leading exponent is compatible with the value $1/6$ but our statistical (and systematic) accuracy is not good enough to allow us to rule out the value $1/4$: the main culprits are the data points for large systems (mostly $N = 4096$ and $N = 2048$), and we would need a much larger number of samples to have a precise determination of this exponent from figure 10 only.

In the critical region $\delta F \sim f(tN^{1/3})$, where δF are the sample-to-sample fluctuations of the total free energy [23] and $t = 1 - T/T_c$. The sample-to-sample internal energy fluctuations are related to the t derivative of δF and they scale as $N^{1/3} f(tN^{1/3})$, where $f(x)$ goes like $1/x$ at large negative x, see figure 11, and is a constant at $x = 0$, i.e. $T = T_c$. The scaling is excellent in the paramagnetic phase (on the left) and in the spin glass phase where $tN^{1/3}$ is small, namely before the ∞-RSB effects start to be important, leading to a different behaviour. Figure 11 clearly shows the two scaling regimes. The ∞-RSB effects are only present for $T < T_c$, in the regime where Nt^6 is large [34] so multiple pure states can exist. In the

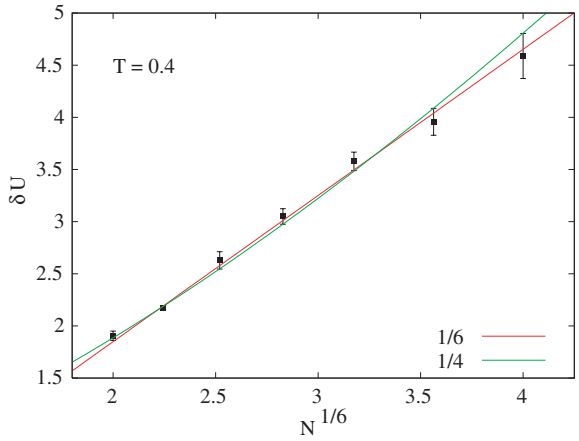

Figure 10. The energy fluctuations $\delta U = N\Delta(T)$ as a function of N, for $T = 0.4$. The two lines are best fits to power laws with exponents $1/6$ and $1/4$ respectively.

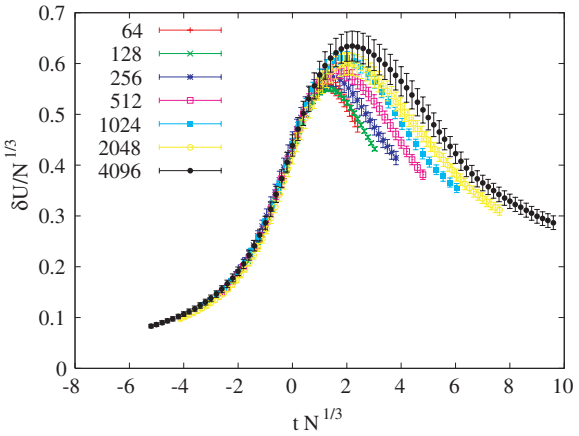

Figure 11. Scaling plot of $\delta U/N^{1/3}$ as a function of $tN^{1/3}$.

finite-size critical regime one has Nt^3 fixed with t going to zero. This makes Nt^6 go to zero, so that in the critical regime RSB effects are absent.

In figure 12, we visualize the scaling behaviour of δU in a different way; we show an effective exponent $1 - \zeta$ obtained from a fit of $x = \delta U/(E(e))$ to the form $\propto N^{1-\zeta}$ as a function of T. This plot is consistent with the guess that the exponent at $T = 0$ takes a value of $1/6$: in order to get a value of $1/4$ we should have a very complex T-dependence of the effective exponent. The situation at $T < T_c$ and exactly at $T = T_c$ is more complicated: it is possible to see that finite-size effects bring down the value of the exponent with increasing lattice size, and a scenario where the true exponent is $1/6$ for all $T < T_c$ (but with large finite-size corrections) is plausible and consistent with the data.

8. The number of pure states

It is useful to consider how the peaks in $P_J(q)$ arise. Suppose we have just two states, state a and its spin reverse A. Then using the definition of $P_J(q)$ in equation (1), if copy 1 is in a

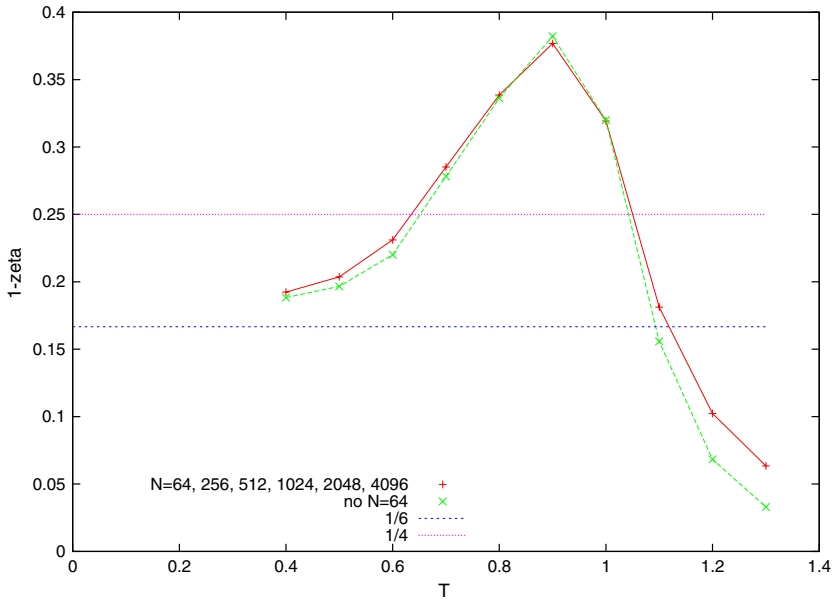

Figure 12. Exponent $1-\zeta$ as a function of T. We show with the continuous lines the results of two best fits, one including all values of N and the other including only values $N \geqslant 128$.

and copy 2 is also in a there will be a peak at $+q_{\mathrm{EA}}$. If both copies are in A, there will also be a peak at $+q_{\mathrm{EA}}$. However, if copy 1 is in state a and copy 2 is in state A, that will produce a peak at $-q_{\mathrm{EA}}$: the same will be true when copy 1 is in state A and copy 2 is in state a.

Suppose now we have four states a, A, b, B. Because (in the infinite volume limit) q_{EA} is the same for all states the overlaps aa, AA, bb, BB are all q_{EA}, and aA, bB, Aa, Bb are all $-q_{\mathrm{EA}}$. The overlaps $ab = q_{12} = AB$, and $aB = -q_{12} = Ab$, giving four peaks in total. (If $q_{12} = 0$ we have three peaks only.) However, the peak at $\pm q_{12}$ will not in general have the same weight as that at q_{EA}.

Then, from the above, two states give two peaks and four states give four peaks (if all involved overlaps are large than zero).

With three states 1, 2 and 3 the effects of the ultrametric organization of states start to play a role. Besides the peak at q_{EA}, there could be overlaps q_{12}, q_{23} and q_{13} making at most four peaks (if all the overlaps are non-zero). But ultrametricity says that either all three q's are equal or two are equal, making at most three peaks (six peaks when one includes the time-reversed states).

With four states $1, 2, 3$ and 4, besides the peak at q_{EA}, there are the overlaps $q_{12}, q_{13}, q_{14}, q_{23}, q_{24}, q_{34}$, but here ultrametricity limits one to three distinct possibilities, making four peaks in total (and eight when one includes the time-reversed states).

There is clearly a pattern here; if states are organized ultrametrically their number is equal to the number of peaks of $P_J(q)$ (plus one if there is a peak at $q = 0$). We are thus predicting that the number of pure states grows with N as $\sim N^{1/6}$. These pure states are those whose total free energy is of order $k_B T$ from that of the lowest free energy state. It is only the overlaps of these low-lying states which can produce detectable features in $P_J(q)$.

Another way of determining the number of pure states at level K is to observe that if one starts from the bottom (the leaves) of a genealogical tree, and moves towards the ancestors,

points that are going up can only meet at the bifurcations of the tree. Hence, the number of overlaps is equal to the number of levels K in the tree.

9. Application to a finite number of dimensions

The exponent Υ which determines the sample-to-sample fluctuations δF of the free energy of the SK model has a significance beyond this model as it appears in the theory of the interface free energy of *finite-dimensional* spin glasses.

In [30] it was shown by going to one-loop order about the Parisi RSB mean-field solution that the variance of the interface free energy associated with the change in the free energy on going from periodic to antiperiodic boundary conditions, $\delta F_{P,\mathrm{AP}} = F_P - F_{\mathrm{AP}}$, is of the form

$$\overline{\delta F_{P,\mathrm{AP}}^2} = L^2 f(L/M) + \overline{\delta F^2}. \tag{19}$$

Here the system is of length L in the z-direction, and it is periodic and of length M in the transverse $d-1$ dimensions. The change from periodic to anti-periodic boundary conditions is done by flipping the sign of the bonds in a hyperplane perpendicular to the z-axis. It follows that $\overline{\delta F_{P,AP}} = 0$. $\overline{\delta F^2}$ is the bond-averaged variance of the free energy of the SK model containing $N = LM^{d-1}$ spins. Equation (19) is valid at least to one-loop order, and its form is probably unchanged whenever the loop expansion is possible; the loop expansion is well defined in the low-temperature spin glass state when $d > 6$, but its existence is problematic for $d < 6$ (see [4]).

The first term in equation (19) is of the standard aspect-ratio scaling form [35, 36], where the zero-temperature scaling exponent θ is equal to 1. When L is of order M, $\overline{\delta F^2}$ is of order $N^{2\Upsilon}$, i.e. of order $\sim L^{d/3}$ if $\Upsilon = 1/6$. This term is not of the standard aspect-ratio scaling form; it depends instead on the total number of spins in the system. This reflects the fact that in RSB situations domain walls have a fractal dimension d_s equal to d, i.e. they are space filling. For example in dimension $d = 2$, where we know that we do not have a broken symmetry phase, domain walls are fractal with $d_s < d$. The variance of the interface free energy is *dominated* by the SK-like term for all $d > 6$ provided that $\Upsilon = 1/6$. If $\Upsilon = 1/6$, one would expect that numerical studies of the defect energy in six dimensions would suggest a value of θ close to unity; exactly in $d = 6$ Boettcher [32] found that $\theta \approx 1.1 \pm 0.1$. In $d = 7$, it is reported in [33] that $\theta \approx 1.244 \pm 0.05$, also compatible with $d/6$. It is possible that when $d < 6$ the standard aspect-ratio scaling form will dominate. (Of course, when $d < 6$, the one-loop expression for the interface free energy will no longer be adequate.) Thus, the dominant term in the L-dependence of the interface free energy could have very different forms above and below six dimensions; note that $d = 6$ plays a special role only if the exponent Υ is exactly $1/6$.

For $d < 6$ the loop expansion about the Parisi RSB state becomes problematical but it is clearly possible that the essential features of RSB might survive even in $d < 6$ and that the appropriate analytic approach could allow us to make that clear. Another possibility is that for $d < 6$ the droplet picture of spin glasses [37, 38] would apply instead, as advocated in [5], so that the nature of the spin glass state would change from being RSB like for $d > 6$ to being replica symmetric for $d < 6$. According to this picture $P_J(q)$ should become just two delta functions at $\pm q_{\mathrm{EA}}$ in the thermodynamic limit, corresponding to just a state and its time reverse. (In fact, for finite systems in three dimensions, $P_J(q)$ appears strikingly similar to that of the finite N SK model [39]. Unfortunately, no systematic study has been made as to how the number of peaks, humps and shoulders evolves with system size; such an investigation could be very informative as regards the true nature of the three-dimensional spin glass state.)

We have argued here that for the finite N SK model the replica-symmetry breaking is stabilized at a finite value of K by self-energy effects. The replica symmetric state of the droplet picture corresponds to having $K = 1$. Thus were the droplet picture to be the valid description of spin glasses below six dimensions (and some of the authors of this paper would argue that this is unlikely!), the same mechanism could stabilize the replica symmetric state. While perturbatively there seems to be no way that the replica symmetric state could be stable, it is possible that if the full self-energy corrections about that state could be included into the calculation, then replica symmetry might be maintained [5].

Acknowledgments

We thank Giorgio Parisi for interesting verbal and virtual conversations about many of the topics discussed in this paper. We thank Marc Mézard for useful comments and advice, and Jean-Philippe Bouchaud for discussions. We also thank Andrea Crisanti and Tommaso Rizzo for their numerical results.

Appendix A. The N-dependence of the self-energy

In this appendix we shall estimate the N-dependence of the self-energy Σ_R. This is needed for our argument that the number of features R scale as $N^{1/6}$. A direct calculation of Σ_R would be impractical: it would involve summing diagrams to all orders. Because of that we will obtain the N-dependence of Σ_R indirectly via a study of the TAP equations [40] of the model.

The TAP equations provide a non-replica way of finding single-valley correlations. For the magnetization m_i at site i within a single state they give

$$m_i = \tanh\left(\beta \sum_j J_{ij} m_j - \beta m_i \sum_j J_{ij}^2 \left(1 - m_j^2\right) + \beta h_i\right). \tag{A.1}$$

The spin glass susceptibility is defined as

$$\chi_{\mathrm{SG}} \equiv \frac{1}{N} \sum_{i,j} \left(\frac{\partial m_i}{\partial \beta h_j}\right)^2. \tag{A.2}$$

When the right-hand side is bond-averaged over the exchange interactions J_{ij} we obtain $G_R(0)$. In the following we will only consider the case of zero magnetic field, $h_i = 0$.

It is convenient to express χ_{SG} in terms of the eigenvalues of the Hessian matrix of the second derivatives of the TAP free energy [41]:

$$A_{ij} \equiv \partial^2(\beta F_{\mathrm{TAP}})/\partial m_i \partial m_j = -2\beta^2 J_{ij}^2 m_i m_j - \beta J_{ij} + \left(\beta^2 \sum_k J_{ik}^2 \left(\left(1 - m_k^2\right) + \left(1 - m_i^2\right)^{-1}\right)\right) \delta_{ij}. \tag{A.3}$$

In terms of the eigenvalues λ of $\mathbf{A}$,

$$\chi_{\mathrm{SG}} = \frac{1}{N} \sum_{\lambda} \frac{1}{\lambda^2}, \tag{A.4}$$

which in terms of the density of states $\rho(\lambda)$ becomes

$$\chi_{\mathrm{SG}} = \lim_{N\to\infty} \int_{\lambda_{\min}}^{\infty} \mathrm{d}\lambda \rho(\lambda)/\lambda^2. \tag{A.5}$$

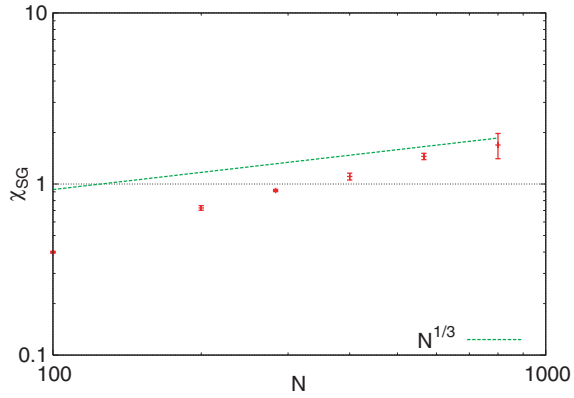

Figure A1. The spin glass susceptibility χ_{SG} as a function of the system size appears to grow faster than the predicted $N^{1/3}$. This is due to finite-size effects, see the text.

The first term on the right-hand side of equation (A.3) is of order $1/N$ and is smaller than the other terms which are either of order $1/N^{1/2}$ or, on the diagonal, of order 1. It will be dropped. (We are focusing in this work on the low-lying TAP states—the pure states—where the mechanism for splitting off an isolated eigenvalue as in [42] cannot operate.) A stable solution of the TAP equations which corresponds to a minimum requires all the eigenvalues of the matrix **A** to be positive. For pure states, $\rho(\lambda)$ is non-zero right to the origin; at small λ (see [41]) one has that

$$\rho(\lambda) = \frac{1}{\pi}\left(\frac{T}{T_c}\right)^3 \left[\frac{1}{N}\sum_i \left(1-m_i^2\right)^3\right]^{-1/2} \lambda^{\frac{1}{2}}. \tag{A.6}$$

With this form for $\rho(\lambda)$, the integral in equation (A.5) would be divergent without its lower cutoff at $\lambda_{\min}$. The N-dependence of $\lambda_{\min}$ itself can be estimated by setting

$$1 = N\int_0^{\lambda_{\min}} \mathrm{d}\lambda \rho(\lambda), \tag{A.7}$$

which means that $\lambda_{\min} \sim N^{-2/3}$. Using this result, we can estimate the N-dependence of χ_{SG} as $N^{1/3}$ using equation (A.5). Note that this result would also apply at T_c.

In fact there is a very simple direct argument for the behaviour at T_c. According to [5, 12] for $T > T_c$,

$$\chi_{SG} = \frac{1}{|t|} f(N|t|^3), \tag{A.8}$$

so that as $|t|$ goes to zero, that is, at T_c, $\chi_{SG} \sim N^{1/3}$.

We would not expect that bond-averaging χ_{SG} to get $G_R(0)$ will modify this N-dependence since single-valley quantities are expected to be self-averaging.

Thus for $T \leqslant T_c$, the single-valley spin glass susceptibility $G_R(0)$ diverges as $N^{1/3}$. This implies that the typical value of K, the order of replica-symmetry breaking in a finite system of N spins, will be via equation (6) of order $tN^{1/6}$. The data in figure 1 are clearly consistent with this expectation.

We have numerically tested the prediction $\chi_{SG} \sim N^{1/3}$ using the iteration procedure described in [43]. This method allows us to find many TAP states even for large system sizes (see [43] for a discussion of the proximity of the iteration algorithm to a dynamical critical point and the influence of this on the free energy of the states found—here we chose the

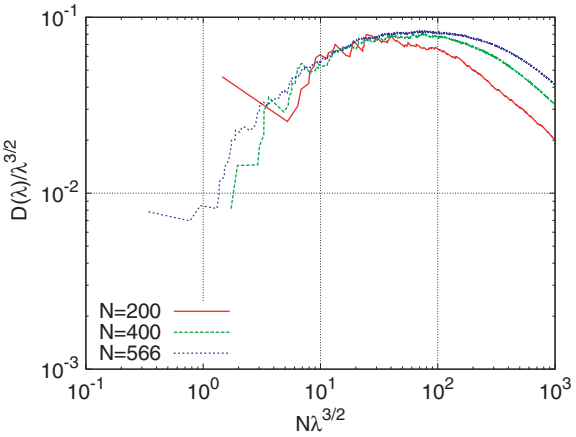

Figure A2. Scaling plot of the averaged integrated density of states of the Hessians for different system sizes.

proximity for each system size in such a way that we get the same free energy range for all system sizes). Using systems with $N = 100, 200, 283, 400, 566$ and 800 at a temperature of $T = 1.0/\beta = 0.2$, we have calculated the Hessian for every state found. The diagonalization of the Hessians was done using arbitrary precision arithmetic (with an accuracy of 50 decimal digits) since these matrices are extremely ill-conditioned and so they are hard to diagonalize: standard packages, for instance the LAPACK routines, fail at the task. The eigenvalues were used to calculate χ_{SG} as in equation (A.4). The results are shown in figure A1.

Surprisingly, χ_{SG} appears to grow faster than $N^{1/3}$. We believe, however, that this is a finite-size effect. To back up this claim, we show in figure A2 a scaling plot of the averaged integrated eigenvalue density $D(\lambda)$ of the Hessians of sizes $N = 200$, 400 and 566.

The expectation is that in the thermodynamic limit this function goes as $D(\lambda) = D_\infty(\lambda) \sim \lambda^{3/2}$ for small λ (corresponding to $\rho(\lambda) \sim \lambda^{1/2}$). For finite N there is a cutoff around $\lambda \approx N^{-2/3}$. The natural expectation is that this cutoff is of the form $D(\lambda) = D_\infty(\lambda) f(N\lambda^{3/2})$ with a scaling function $f(x)$. This is verified in figure A2. The arguments sketched above which lead to the prediction $\chi_{\mathrm{SG}} \sim N^{1/3}$ for large N can only be expected to be valid when the interval in which $D(\lambda) \approx \lambda^{3/2}$ prevails is large enough. This interval can be identified as the horizontal (or nearly horizontal) stretch in figure A2. Clearly, this interval is very small as it is not even one decade for the available system sizes. The conclusion is, therefore, that we cannot yet expect to see the asymptotic scaling behaviour. It is not possible to go to larger system sizes as the arbitrary precision diagonalization of the Hessians becomes computationally too expensive.

Appendix B. Free energy fluctuations and $J(p)$

According to [11], the exact expression for the quantity $J(p)$ for a finite number of replica-symmetry breaking steps K and for the truncated model with Hamiltonian

$$\mathcal{H} = -\frac{t}{2}\sum_{\alpha,\beta} q_{\alpha\beta}^2 - \frac{w}{6}\sum_{\alpha,\beta,\gamma} q_{\alpha\beta}q_{\beta\gamma}q_{\gamma\alpha} - \frac{y}{12}\sum_{\alpha,\beta} q_{\alpha\beta}^4 \tag{B.1}$$

is

$$J(p) = -\sum_{k,l=1}^{K+1} \mu_0(k)\mu_0(l)\log(p^2 + \lambda(0;k,l)), \tag{B.2}$$

where

$$\mu_r(k) = \begin{cases} \dfrac{1}{p_k} - \dfrac{1}{p_{k-1}} & k > r-1 \\ \dfrac{1}{p_{r+1}} & k = r+1 \end{cases}, \tag{B.3}$$

$$p_k = \frac{2y}{w} q_K \frac{k-\frac{1}{2}}{K}, \tag{B.4}$$

$$\lambda(r;k,l) = 2y\frac{q_K^2}{K^2}\left(\frac{1}{2}(k-1)^2 + \frac{1}{2}(l-1)^2 - r^2 - \frac{1}{6}\right), \tag{B.5}$$

and q_K is the solution of

$$t - wq_K + y\left(1 - \frac{1}{6K^2}\right)q_K^2 = 0. \tag{B.6}$$

When the expressions for $\mu_r(k)$ and $\mu_r(l)$ are inserted, equation (B.2) can be rewritten as

$$J(p) = -2\sum_{k=1}^{K}\frac{1}{p_k}\log\frac{p^2+\lambda(0;k,K+1)}{p^2+\lambda(0;k+1,K+1)} - \log(p^2+\lambda(0;K+1,K+1)) - \sum_{k,l=1}^{K}\frac{1}{p_k p_l}\log\left(\frac{p^2+\lambda(0;k,l)}{p^2+\lambda(0;k+1,l)}\frac{p^2+\lambda(0;k+1,l+1)}{p^2+\lambda(0;k,l+1)}\right). \tag{B.7}$$

We are interested in the behaviour for small p where $J(p)$ diverges as p approaches $\frac{yq_K^2}{3K^2}$. It is easy to see that the first two terms of the former expression are well behaved in this limit. The divergence in p must therefore come from the last term, which will be denoted by $\hat{J}(p)$. Defining

$$x^2 = \frac{K^2p^2}{yq_K^2} - \frac{1}{3} \tag{B.8}$$

and renumbering the sums to start from 0 it can be cast in the form

$$\hat{J}(p) = -\frac{w^2\left(x^2+\frac{1}{3}\right)}{4yp^2}\sum_{k,l=0}^{K-1}\frac{1}{\left(k+\frac{1}{2}\right)\left(l+\frac{1}{2}\right)} \times \log\left(\frac{x^2+k^2+l^2}{x^2+(k+1)^2+l^2}\frac{x^2+(k+1)^2+(l+1)^2}{x^2+k^2+(l+1)^2}\right). \tag{B.9}$$

While p was a finite-dimensional wave vector in [11], here we consider it as a proxy for the self-energy as we are dealing with the SK model. Substituting $\Sigma_R = cN^{-1/3}$ for p^2 and making the usual replacement $K = c'tN^{1/6}$ (where the constant c' is large enough to guarantee stability) yields (to leading order in N) $x^2 = \frac{c'^2ct^2}{yq_\infty^2} - \frac{1}{3}$ and $\hat{J} = \delta F^2 = N^{1/3}f(t)$. The function $f(t)$ is defined by the remaining prefactors and the sums (with upper bounds set to infinity) in equation (B.9). This shows that the typical sample-to-sample fluctuations of the free energy are of order $N^{1/6}$.

References

[1] Sherrington D and Kirkpatrick S 1975 *Phys. Rev. Lett.* **35** 1792
[2] Parisi G 1980 *J. Phys. A: Math. Gen.* **13** L115

[3] Talagrand M 2003 *Spin Glasses: A Challenge for Mathematicians. Mean Field Theory and Cavity Method* (Berlin: Springer)
[4] De Dominicis C, Kondor I and Temesvári T 1997 *Spin Glasses and Random Fields* ed A P Young (London: World Scientific) (see also *Preprint* cond-mat/9705215)
[5] Moore M A 2005 *J. Phys. A: Math. Gen.* **38** L783
[6] Janiš V and Klíč A 2006 *Phys. Rev.* B **74** 054410
[7] Oppermann R, Schmidt M J and Sherrington D 2007 *Phys. Rev. Lett.* **98** 127201
[8] Billoire A 2006 *Phys. Rev.* B **73** 132201
[9] Billoire A, Franz S and Marinari E 2003 *J. Phys. A: Math. Gen.* **36** 15
[10] Aspelmeier T and Moore M A 2003 *Phys. Rev. Lett.* **90** 177201
[11] De Dominicis C and Di Francesco P 2003 *J. Phys. A: Math. Gen.* **36** 10955
[12] Yeo J, Moore M A and Aspelmeier T 2005 *J. Phys. A: Math. Gen.* **38** 4027
[13] Billoire A and Marinari E 2000 *J. Phys. A: Math. Gen.* **33** L265
[14] Billoire A and Marinari E 2002 *Europhys. Lett.* **60** 775
[15] Berg B A and Janke W 1998 *Phys. Rev. Lett.* **80** 4771
[16] Berg B A, Billoire A and Janke W 2000 *Phys. Rev.* B **61** 12143
[17] Crisanti A and Rizzo T 2006 *Phys. Rev.* E **65** 046137 and private communication
[18] Katzgraber H G and Campbell I A 2003 *Phys. Rev.* B **68** 180402(R)
[19] Billoire A 2007 *Rugged Free Energy Landscapes (Springer Lecture Notes in Physics)* ed W Janke (Berlin: Springer)
[20] Boettcher S 2005 *Eur. Phys. J.* B **46** 501
[21] Boettcher S 2003 *Eur. Phys. J.* B **31** 29
[22] Cabasino S, Marinari E, Paolucci P and Parisi G 1988 *J. Phys. A. Math Gen* **21** 4201
[23] Crisanti A, Paladin G, Sommers H-J and Vulpiani A 1992 *J. Phys. I France* **2** 1325
[24] Parisi G and Rizzo T 2007 *Preprint* 0706.1180
[25] Palassini M 2000 *PhD Thesis*, Scuola Normale Superiore di Pisa (unpublished)
[26] Palassini M 2003 *Preprint* cond-mat/0307713
[27] Bouchaud J-P, Krzakala F and Martin O 2003 *Phys. Rev.* B **68** 224404
[28] Katzgraber H G, Körner M, Liers F, Jünger M and Hartmann A K 2005 *Phys. Rev.* B **72** 094421
[29] Pál K 2006 *Physica* A **367** 261
[30] Aspelmeier T, Moore M A and Young A P 2003 *Phys. Rev. Lett.* **90** 127202
[31] Aspelmeier T 2007 *Phys. Rev. Lett.* at press (*Preprint* 0712.3586)
[32] Boettcher S 2004 *Eur. Phys. J.* B **38** 83
[33] Boettcher S 2004 *Europhys. Lett.* **67** 453
[34] Bray A J and Moore M A 1980 *J. Phys. C: Solid State Phys.* **13** L469
[35] Carter A C, Bray A J and Moore M A 2002 *Phys. Rev. Lett.* **88** 0277201
[36] Hartmann A K, Bray A J, Carter A C, Moore M A and Young A P 2002 *Phys. Rev.* B **66** 224401
[37] Bray A J and Moore M A 1987 *Lect. Notes Phys.* **275** 121
[38] Fisher D S and Huse D A 1988 *Phys. Rev.* B **38** 386
[39] Parisi G 2007 *Preprint* 0706.0094
[40] Thouless D J, Anderson P W and Palmer R G 1977 *Phil. Mag.* **35** 593
[41] Bray A J and Moore M A 1979 *J. Phys. C: Solid State Phys.* **12** L441
[42] Aspelmeier T, Bray A J and Moore M A 2004 *Phys. Rev. Lett.* **92** 087203
[43] Aspelmeier T, Blythe R, Bray A J and Moore M A 2006 *Phys. Rev.* B **74** 184411